Journal of Systems Engineering and Electronics
Vol. 33, No. 1, February 2022, pp.180 – 187

Civil aircraft fault tolerant attitude tracking based on extended state observers and nonlinear dynamic inversion

MA Xinjian, LIU Shiqian*, and CHENG Huihui

School of Aeronautics and Astronautics, Shanghai Jiao Tong University, Shanghai 200240, China

Abstract: For the problem of sensor faults and actuator faults in aircraft attitude control, this paper proposes a fault tolerant control (FTC) scheme based on extended state observer (ESO) and nonlinear dynamic inversion (NDI). First, two ESOs are designed to estimate sensor faults and actuator faults respectively. Second, the angular rate signal is reconstructed according to the estimation of sensor faults. Third, in angular rate loop, NDI is designed based on reconstruction of angular rate signals and estimation of actuator faults. The FTC scheme proposed in this paper is testified through numerical simulations. The results show that it is feasible and has good fault tolerant ability.

Keywords: fault tolerant control (FTC), signal reconstruction, extended state observer (ESO), nonlinear dynamic inversion (NDI).

DOI: 10.23919/JSEE.2022.000018

1. Introduction

To ensure flight safety of civil aircrafts, fault tolerant control (FTC) are designed to handle faults of important sensors and actuators. Typical researches on actuator FTC are conducted [1−9]. Alwi et al. used a sliding mode observer (SMO) to estimate actuator fault [1,2], and Quan applied this method on flight control [3], but this method was only suitable for systems with linear observable terms. Lu et al. proposed an incremental nonlinear dynamic inversion (NDI) control to realize fault tolerant trajectory tracking [4], and Cheng et al. combined incremental NDI with neural network to deal with actuator fault and pilot mishandling simultaneously [5]. However, this method had heavy work load on parameter adjustment.Leeetal.usedanunknowninputobservertodetectactuator fault [6], but this method was also based on the linearized system. Yu et al. combined fuzzy neural networks and sliding mode controller to realize the FTC [7], but this method involved complex calculation. Wang et al. used stable inversion on fault tolerant auto landing of civil aircrafts [8], but it did not solve the problem of nonlinearity. Liu et al. proposed a sliding mode backstepping to do trajectory FTC [9] based on a nonlinear aircraft. In order to deal with the nonlinearity, recently, researchers have been working on actuator FTC by using extended state observer (ESO) [10−17]. On behalf of these researches, Yuan et al. combined ESO with NDI to improve the control robustness [16], and Falconi et al. further realized FTC through this method [17]. Theoretical analysis of ESO were given in [18,19]. These ESO-based FTC methods were designed to solve the problem of nonlinearity.

However, few of these researches mentioned above involved the sensor faults. Hence, in order to solve the problems of sensor faults, Edwards et al. proposed an SMO-based fault detection method for sensor faults [20], and Xia et al. proposed an observer-based signal reconstruction method [21], but they were only suitable for the linear system. Johansen et al. proposed an airflow angle estimation method which can be used when airflow angle sensor have faults [22], but its accuracy still needs to be improved. Li et al. used Kalman filter to do the signal estimation under white noise [23], but this method has difficulty dealing with bias sensor fault. Chen et al. proposed a nonlinear adaptive observer-based sensor FTC scheme [24]. Yang et al. proposed a fault diagnosis method for angle-of-attack based on the transfer function of linear model [25], but this method has difficulty dealing with nonlinear systems. Lu et al. proposed a sensor fault detection method in [26,27] and developed an FTC scheme for simultaneous fault of sensors and actuators by decoupling design [28]. However, Lu's method needs sophisticated parameter adjustment. Generally, most of these methods either have difficulty dealing with nonlinear systems or need complex calculation. Therefore, how to solve simultaneous sensor and actuator faults in an

Manuscript received December 22, 2020.
*Corresponding author.
This work was supported by the Chinese Aviation Science Fund (20160757001) and the National Natural Science Foundation of China (10577012).

easy way has become a heated topic.

The control scheme of [16] and [17] based on NDI and ESO has a good performance on actuator FTC. However, neither of them has taken sensor faults into consideration. Thus, motivated by the work of [16] and [17], this paper further improves the control law design so that it can deal with actuator faults and sensor faults simultaneously. First, two ESOs are designed to estimate sensor faults and actuator faults respectively. Second, the angular rate signal is reconstructed according to the estimation of sensor faults. Third, the NDI in angular rate loop is designed based on the reconstruction of angular rate signals and the estimation of actuator faults. Finally, another NDI is designed to realize the attitude tracking. The proposed FTC scheme is verified through simulations. The results show that it is feasible and has better fault tolerant ability than conventional ESO-NDI design.

Main innovation and contribution of this paper can be summarized as follows:

(i) To solve the problem of sensor faults, this paper proposes a novel ESO-based sensor fault estimation method and realizes the reconstruction of aircraft angular rate signal using a nonlinear aircraft model.

(ii) Conventional ESO-NDI design has difficulty dealing with simultaneous sensor and actuator faults. To overcome this weakness, the FTC is modified, and the fault tolerant attitude control of an aircraft is realized with simultaneous sensor and actuator faults.

This paper is organized as follows: Section 2 gives the aircraft model; Section 3 gives the design of ESO and NDI; Section 4 gives some simulations on a Cessna172 aircraft model; Section 5 presents conclusions.

2. Problem formulation

The aircraft attitude control scheme includes an attitude angle control loop and an angular rate control loop, as shown in Fig. 1, where $\boldsymbol{\omega}$ and $\boldsymbol{\eta}$ denote the angular rate and attitude vector respectively, the associated commands are $\boldsymbol{\omega}_c$ and $\boldsymbol{\eta}_c$, and measurements are $\boldsymbol{\omega}_m$ and $\boldsymbol{\eta}_m$ respectively. $\boldsymbol{u}_c$ and $\boldsymbol{u}$ are command and actual inputs of actuators.

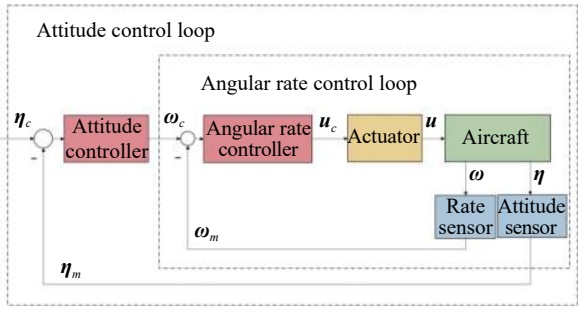

Fig. 1 Attitude control scheme

According to [29], the angular rate dynamics of aircraft is presented as follows:

$$\begin{cases} \dot{p} = \dfrac{I_{xz}(I_{xx}-I_{yy}+I_{zz})}{I_{xx}I_{zz}-I_{xz}^2}pq + \dfrac{I_{zz}(I_{yy}-I_{zz})-I_{xz}^2}{I_{xx}I_{zz}-I_{xz}^2}qr + \\ \qquad \dfrac{I_{zz}}{I_{xx}I_{zz}-I_{xz}^2}L + \dfrac{I_{xz}}{I_{xx}I_{zz}-I_{xz}^2}N \\ \dot{q} = \dfrac{I_{zz}-I_{xx}}{I_{yy}}pr + \dfrac{I_{xz}}{I_{yy}}\left(r^2-p^2\right) + \dfrac{1}{I_{yy}}M \\ \dot{r} = \dfrac{I_{xx}(I_{xx}-I_{yy})+I_{xz}^2}{I_{xx}I_{zz}-I_{xz}^2}pq + \dfrac{I_{xz}(I_{yy}-I_{xx}-I_{zz})}{I_{xx}I_{zz}-I_{xz}^2}pr + \\ \qquad \dfrac{I_{xz}}{I_{xx}I_{zz}-I_{xz}^2}L + \dfrac{I_{xx}}{I_{xx}I_{zz}-I_{xz}^2}N \end{cases} \tag{1}$$

where p, q, and r represent the roll, pitch, and yaw rate of the aircraft respectively. L, M, and N represent the roll, pitch, and yaw moments of the aircraft. I_{xx}, I_{yy}, I_{zz}, and I_{xz} are the moments of inertia of the aircraft. Denote $\boldsymbol{\omega} = \begin{bmatrix} p & q & r \end{bmatrix}^{\mathrm{T}}$ as the state vector of angular rate loop.

Assume that the moments on the aircraft are only generated by aerodynamic force, which means the moments generated by thrust are ignored. Hence, the aerodynamic moments can be calculated as follows:

$$\begin{bmatrix} L \\ M \\ N \end{bmatrix} = \boldsymbol{R}_{bw} \cdot \left(\bar{q}S \begin{bmatrix} b \cdot C_L \\ \bar{c} \cdot C_M \\ b \cdot C_N \end{bmatrix} + \bar{q}S \begin{bmatrix} C_D \\ C_Y \\ C_l \end{bmatrix} \times \Delta \boldsymbol{l} \right) \tag{2}$$

where $\boldsymbol{R}_{bw}$ is the coordinate transform matrix from wind frame to body frame. The transform matrix can be found in [29]. $\bar{q}$ is the dynamic pressure, S is wing reference area, b is wing span, $\bar{c}$ is the mean aerodynamic chord. C_L, C_M, and C_N are aerodynamic moment coefficients, C_D, C_Y, and C_l are aerodynamic coefficients of drag, lateral and lift force in wind frame respectively. And $\Delta \boldsymbol{l}$ is the distance vector from pressure center to gravity center that can be described as follows:

$$\Delta \boldsymbol{l} = \boldsymbol{R}_{wb} \cdot \begin{bmatrix} x_{cg} - x_{cp} \\ 0 \\ 0 \end{bmatrix} = \boldsymbol{R}_{bw}^{\mathrm{T}} \cdot \begin{bmatrix} x_{cg} - x_{cp} \\ 0 \\ 0 \end{bmatrix} \tag{3}$$

where $\boldsymbol{R}_{wb}$ is the transform matrix from body frame to wind frame, and x_{cg} and x_{cp} are the position of gravity center and pressure center along x axis in body frame.

The aerodynamic moment coefficient C_L, C_M, and C_N are coefficients that directly affect angular motion, which can be calculated as follows:

$$\begin{bmatrix} C_L \\ C_M \\ C_N \end{bmatrix} = \begin{bmatrix} C_{L0} \\ C_{M0} \\ C_{N0} \end{bmatrix} + \begin{bmatrix} C_{L\beta} \\ C_{M\alpha} \\ C_{N\beta} \end{bmatrix} + \begin{bmatrix} \dfrac{C_{Lp}b}{2V_t} & 0 & \dfrac{C_{Lr}b}{2V_t} \\ 0 & \dfrac{C_{Mq}\bar{c}}{2V_t} & 0 \\ \dfrac{C_{Np}b}{2V_t} & 0 & \dfrac{C_{Nr}b}{2V_t} \end{bmatrix} \boldsymbol{\omega} + \begin{bmatrix} C_{L\delta_a}b & 0 & C_{L\delta_r}b \\ 0 & C_{M\delta_e}\bar{c} & 0 \\ C_{N\delta_a}b & 0 & C_{N\delta_r}b \end{bmatrix} \begin{bmatrix} \delta_a \\ \delta_e \\ \delta_r \end{bmatrix} \tag{4}$$

where C_{L0}, C_{M0}, and C_{N0} are the constant parts of aerodynamic moment coefficient. $C_{L\beta}$, $C_{M\alpha}$, and $C_{N\beta}$ are aerodynamic moment coefficients generated by airflow angles. V_t is the true airspeed. C_{Lp}, C_{Np}, C_{Mq}, C_{Lr}, and C_{Nr} are aerodynamic moment derivatives. $C_{L\delta_a}$, $C_{N\delta_a}$, $C_{N\delta_e}$, $C_{L\delta_r}$, and $C_{N\delta_r}$ are control surface related derivatives, δ_a, δ_e, and δ_r are the deflection of aileron, elevator, and rudder, respectively. Denote $\boldsymbol{u} = \begin{bmatrix} \delta_a & \delta_e & \delta_r \end{bmatrix}^{\mathrm{T}}$ as the input to aircraft. Substituting (2) and (4) into (1) yields

$$\dot{\boldsymbol{\omega}} = \boldsymbol{F}_1(\boldsymbol{\omega}) + \boldsymbol{G}_1(\boldsymbol{\omega})\boldsymbol{u} \tag{5}$$

where $\boldsymbol{F}_1(\boldsymbol{\omega})$ and $\boldsymbol{G}_1(\boldsymbol{\omega})$ are nonlinear functions that can be described as follows:

$$\boldsymbol{F}_1(\boldsymbol{\omega}) = \boldsymbol{F}_{01} + \bar{q}S \cdot \boldsymbol{M}_I \boldsymbol{R}_{bw} \cdot \begin{bmatrix} b(C_{L0} + C_{L\beta}) \\ \bar{c}(C_{M0+}C_{M\alpha}) \\ b(C_{N0} + C_{N\beta}) \end{bmatrix} + \bar{q}S \cdot \boldsymbol{M}_I \boldsymbol{R}_{bw} \cdot \left(\begin{bmatrix} C_D \\ C_Y \\ C_l \end{bmatrix} \times \Delta \boldsymbol{l} + \boldsymbol{M}_\omega \cdot \boldsymbol{\omega} \right), \tag{6}$$

$$\boldsymbol{G}_1(\boldsymbol{\omega}) = \bar{q}S \cdot \boldsymbol{M}_I \boldsymbol{R}_{bw} \boldsymbol{M}_{\boldsymbol{u}}. \tag{7}$$

$\boldsymbol{F}_{01}$, $\boldsymbol{M}_I$, $\boldsymbol{M}_{\boldsymbol{\omega}}$, and $\boldsymbol{M}_{\boldsymbol{u}}$ are described as follows:

$$\boldsymbol{F}_{01} = \begin{bmatrix} \dfrac{I_{xz}(I_{xx} - I_{yy} + I_{zz})}{I_{xx}I_{zz} - I_{xz}^2} pq + \dfrac{I_{zz}(I_{yy} - I_{zz}) - I_{xz}^2}{I_{xx}I_{zz} - I_{xz}^2} qr \\ \dfrac{I_{zz} - I_{xx}}{I_{yy}} pr + \dfrac{I_{xz}}{I_{yy}}\left(r^2 - p^2\right) \\ \dfrac{I_{xx}(I_{xx} - I_{yy}) + I_{xz}^2}{I_{xx}I_{zz} - I_{xz}^2} pq + \dfrac{I_{xz}(I_{yy} - I_{xx} - I_{zz})}{I_{xx}I_{zz} - I_{xz}^2} pr \end{bmatrix}, \tag{8}$$

$$\boldsymbol{M}_I = \begin{bmatrix} \dfrac{I_{zz}}{I_{xx}I_{zz} - I_{xz}^2} & 0 & \dfrac{I_{xz}}{I_{xx}I_{zz} - I_{xz}^2} \\ 0 & \dfrac{1}{I_{yy}} & 0 \\ \dfrac{I_{xz}}{I_{xx}I_{zz} - I_{xz}^2} & 0 & \dfrac{I_{xx}}{I_{xx}I_{zz} - I_{xz}^2} \end{bmatrix}, \tag{9}$$

$$\boldsymbol{M}_{\omega} = \begin{bmatrix} \dfrac{C_{Lp}b^2}{2V_t} & 0 & \dfrac{C_{Lr}b^2}{2V_t} \\ 0 & \dfrac{C_{Mq}\bar{c}^2}{2V_t} & 0 \\ \dfrac{C_{Np}b^2}{2V_t} & 0 & \dfrac{C_{Nr}b^2}{2V_t} \end{bmatrix}, \tag{10}$$

$$\boldsymbol{M}_{\boldsymbol{u}} = \begin{bmatrix} C_{L\delta_a}b & 0 & C_{L\delta_r}b \\ 0 & C_{M\delta_e}\bar{c} & 0 \\ C_{N\delta_a}b & 0 & C_{N\delta_r}b \end{bmatrix}. \tag{11}$$

Since sensor and actuator faults may occur in the angular rate control loop, the angular rate loop can be described as follows:

$$\begin{cases} \dot{\boldsymbol{\omega}} = \boldsymbol{F}_1(\boldsymbol{\omega}) + \boldsymbol{G}_1(\boldsymbol{\omega})(\boldsymbol{u}_c + \boldsymbol{f}_a) \\ \boldsymbol{\omega}_m = \boldsymbol{\omega} + \boldsymbol{f}_s \end{cases} \tag{12}$$

where $\boldsymbol{f}_a$ is actuator fault, which means the difference between actual deflection and desired deflection of aileron, elevator and rudder. $\boldsymbol{f}_s$ is sensor fault, which means the difference between angular rate sensor measurements and true value. $\boldsymbol{u}_c$ is the command of control input, $\boldsymbol{u}$ is the eventual input ($\boldsymbol{u} = \boldsymbol{u}_c + \boldsymbol{f}_a$), and $\boldsymbol{\omega}_m$ is measurement value of angular rate.

The attitude control loop uses Euler angles to describe the attitude. Denote $\boldsymbol{\eta} = \begin{bmatrix} \varphi & \theta & \psi \end{bmatrix}^{\mathrm{T}}$ as the state vector for the attitude loop, where φ, θ, and ψ are the roll, pitch, and yaw angle respectively. Attitude dynamics can be described as (13) according to [29]

$$\dot{\boldsymbol{\eta}} = \boldsymbol{G}_2(\boldsymbol{\eta})\boldsymbol{\omega} \tag{13}$$

where

$$\boldsymbol{G}_2(\boldsymbol{\eta}) = \begin{bmatrix} 1 & \sin\phi \cdot \tan\theta & \cos\phi \cdot \tan\theta \\ 0 & \cos\phi & -\sin\phi \\ 0 & \sin\phi/\cos\theta & \cos\phi/\cos\theta \end{bmatrix}. \tag{14}$$

Assume that there are no sensor faults in attitude variables. Hence, the attitude loop can be described as

$$\begin{cases} \dot{\boldsymbol{\eta}} = \boldsymbol{G}_2(\boldsymbol{\eta})\boldsymbol{\omega} \\ \boldsymbol{\eta}_m = \boldsymbol{\eta} \end{cases} \tag{15}$$

where $\boldsymbol{\eta}_m$ is the measurement of the attitude variables.

3. FTC design based on ESO and NDI

The FTC design includes four parts. ESO_s is for sensor fault estimation, while ESO_a is for actuator fault estimation. $\mathrm{NDI}_{\boldsymbol{\omega}}$ is the controller of angular rate loop, while $\mathrm{NDI}_{\boldsymbol{\eta}}$ is the controller of attitude loop, as shown in Fig. 2.

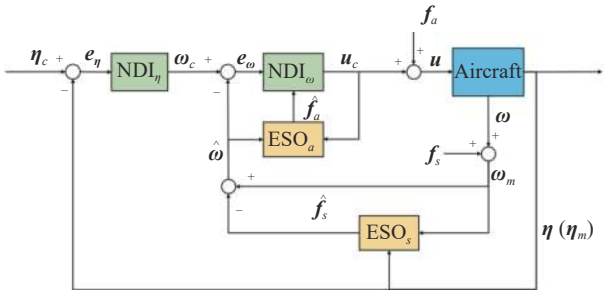

Fig. 2 FTC design based on ESO and NDI

In Fig.2 $\widehat{f_s}$ and $\widehat{f_a}$ are estimation of sensor faults and actuator faults. $\widehat{\omega}$ is the reconstructed angular rate signal. $\boldsymbol{\omega}_c$ and $\boldsymbol{\eta}_c$ are control command of angular rate and attitude angle. $\boldsymbol{e}_\omega$ and $\boldsymbol{e}_\eta$ are the tracking error of angular rate and attitude angle.

3.1 Design of ESO$_s$

ESO$_s$ is used to estimate the sensor faults and reconstruct the angular rate signals. Substitute (12) into (15), and the attitude dynamics can be rewritten as follows:

$$\begin{cases} \dot{\boldsymbol{\eta}} = \boldsymbol{G}_2(\boldsymbol{\eta})(\boldsymbol{\omega}_m - \boldsymbol{f}_s) \\ \boldsymbol{\eta}_m = \boldsymbol{\eta} \end{cases} \tag{16}$$

Denote (16) as System A. Decompose System A into three channels:

$$\begin{cases} \dot{\phi} = \boldsymbol{G}_{21}(\boldsymbol{\eta})\boldsymbol{\omega}_m - \boldsymbol{G}_{21}(\boldsymbol{\eta})\boldsymbol{f}_s \\ \dot{\theta} = \boldsymbol{G}_{22}(\boldsymbol{\eta})\boldsymbol{\omega}_m - \boldsymbol{G}_{22}(\boldsymbol{\eta})\boldsymbol{f}_s \\ \dot{\psi} = \boldsymbol{G}_{23}(\boldsymbol{\eta})\boldsymbol{\omega}_m - \boldsymbol{G}_{23}(\boldsymbol{\eta})\boldsymbol{f}_s \end{cases} \tag{17}$$

where $\boldsymbol{G}_{2i}(\boldsymbol{\eta})$ are the ith row of $\boldsymbol{G}_2(\boldsymbol{\eta})$ (i = 1, 2, 3) .

Denote:

$$\begin{cases} d_\phi = -\boldsymbol{G}_{21}(\boldsymbol{\eta})\boldsymbol{f}_s \\ d_\theta = -\boldsymbol{G}_{22}(\boldsymbol{\eta})\boldsymbol{f}_s \\ d_\psi = -\boldsymbol{G}_{23}(\boldsymbol{\eta})\boldsymbol{f}_s \end{cases} \tag{18}$$

where d_ϕ, d_θ, d_ψ denote the influence of faults in channels of roll, pitch, and yaw respectively.

Design an equivalent system to System A as (19), and denote it as System B

$$\begin{cases} \dot{\zeta}_1 = \zeta_2 + \boldsymbol{G}_{21}(\boldsymbol{\eta})\boldsymbol{\omega}_m \\ \dot{\zeta}_2 = \dot{d}_\phi \\ \dot{\zeta}_3 = \zeta_4 + \boldsymbol{G}_{22}(\boldsymbol{\eta})\boldsymbol{\omega}_m \\ \dot{\zeta}_4 = \dot{d}_\theta \\ \dot{\zeta}_5 = \zeta_6 + \boldsymbol{G}_{23}(\boldsymbol{\eta})\boldsymbol{\omega}_m \\ \dot{\zeta}_6 = \dot{d}_\psi \end{cases} \tag{19}$$

and $\begin{bmatrix} \zeta_1 & \zeta_2 & \zeta_3 & \zeta_4 & \zeta_5 & \zeta_6 \end{bmatrix}^{\mathrm{T}} = \begin{bmatrix} \phi & d_\phi & \theta & d_\theta & \psi & d_\psi \end{bmatrix}^{\mathrm{T}}$. The ESO$_s$ can be designed as follows:

$$\begin{cases} \dot{w}_1 = w_2 + \boldsymbol{G}_{21}(\boldsymbol{\eta})\boldsymbol{\omega}_m - R_{11}(w_1 - \phi) \\ \dot{w}_2 = -R_{12} \cdot \mathrm{sign}(w_1 - \phi) \cdot \sqrt{|w_1 - \phi|} \\ \dot{w}_3 = w_4 + \boldsymbol{G}_{22}(\boldsymbol{\eta})\boldsymbol{\omega}_m - R_{21}(w_3 - \theta) \\ \dot{w}_4 = -R_{22} \cdot \mathrm{sign}(w_3 - \theta) \cdot \sqrt{|w_3 - \theta|} \\ \dot{w}_5 = w_6 + \boldsymbol{G}_{23}(\boldsymbol{\eta})\boldsymbol{\omega}_m - R_{31}(w_5 - \psi) \\ \dot{w}_6 = -R_{32} \cdot \mathrm{sign}(w_5 - \psi) \cdot \sqrt{|w_5 - \psi|} \end{cases} \tag{20}$$

where $\boldsymbol{w} = \widehat{\boldsymbol{\zeta}}$, and $\boldsymbol{R}$ is the observer gain matrix with three rows and two columns. The convergence analysis of ESO are given in [18] and [19].

According to (18), sensor faults can be estimated as

$$\widehat{\boldsymbol{f}_s} = -\boldsymbol{G}_2^{-1}(\boldsymbol{\eta}) \cdot \begin{bmatrix} w_2 & w_4 & w_6 \end{bmatrix}^{\mathrm{T}}. \tag{21}$$

Finally, angular rate signal can be reconstructed as

$$\widehat{\boldsymbol{\omega}} = \boldsymbol{\omega}_m - \widehat{\boldsymbol{f}_s}. \tag{22}$$

3.2 Design of ESO$_a$

ESO$_a$ is designed to estimate actuator faults. Denote (12) as System C, and decompose System C into three channels:

$$\begin{cases} \dot{p} = \boldsymbol{F}_{11}(\boldsymbol{\omega}) + \boldsymbol{G}_{11}(\boldsymbol{\omega})\boldsymbol{u}_c + \boldsymbol{G}_{11}(\boldsymbol{\omega})\boldsymbol{f}_a \\ \dot{q} = \boldsymbol{F}_{12}(\boldsymbol{\omega}) + \boldsymbol{G}_{12}(\boldsymbol{\omega})\boldsymbol{u}_c + \boldsymbol{G}_{12}(\boldsymbol{\omega})\boldsymbol{f}_a \\ \dot{r} = \boldsymbol{F}_{13}(\boldsymbol{\omega}) + \boldsymbol{G}_{13}(\boldsymbol{\omega})\boldsymbol{u}_c + \boldsymbol{G}_{13}(\boldsymbol{\omega})\boldsymbol{f}_a \end{cases} \tag{23}$$

where $\boldsymbol{F}_{1i}(\boldsymbol{\omega})$ and $\boldsymbol{G}_{1i}(\boldsymbol{\omega})$ are the ith row of $\boldsymbol{F}_1(\boldsymbol{\omega})$ and $\boldsymbol{G}_1(\boldsymbol{\omega})$ (i = 1, 2, 3) . Denote:

$$\begin{cases} d_p = \boldsymbol{G}_{11}(\boldsymbol{\eta})\boldsymbol{f}_a \\ d_q = \boldsymbol{G}_{12}(\boldsymbol{\eta})\boldsymbol{f}_a \\ d_r = \boldsymbol{G}_{13}(\boldsymbol{\eta})\boldsymbol{f}_a \end{cases}. \tag{24}$$

where d_p, d_q, d_r are the influence of actuator faults in roll, pitch, and yaw rate channel respectively. Then System D can be designed as an equivalent system to System C:

$$\begin{cases} \dot{\xi}_1 = \xi_2 + \boldsymbol{F}_{11}(\boldsymbol{\omega}) + \boldsymbol{G}_{11}(\boldsymbol{\omega})\boldsymbol{u}_c \\ \dot{\xi}_2 = \dot{d}_p \\ \dot{\xi}_3 = \xi_4 + \boldsymbol{F}_{12}(\boldsymbol{\omega}) + \boldsymbol{G}_{12}(\boldsymbol{\omega})\boldsymbol{u}_c \\ \dot{\xi}_4 = \dot{d}_q \\ \dot{\xi}_5 = \xi_6 + \boldsymbol{F}_{13}(\boldsymbol{\omega}) + \boldsymbol{G}_{13}(\boldsymbol{\omega})\boldsymbol{u}_c \\ \dot{\xi}_6 = \dot{d}_r \end{cases} \tag{25}$$

where $\begin{bmatrix} \xi_1 & \xi_2 & \xi_3 & \xi_4 & \xi_5 & \xi_6 \end{bmatrix}^{\mathrm{T}} = \begin{bmatrix} p & d_p & q & d_q & r & d_r \end{bmatrix}^{\mathrm{T}}$.Then ESO$_a$ can be designed as follows:

$$\begin{cases} \dot{z}_1 = z_2 + \boldsymbol{F}_{11}(\boldsymbol{\omega}) + \boldsymbol{G}_{11}(\boldsymbol{\omega})\boldsymbol{u} - Q_{11}(z_1 - \hat{p}) \\ \dot{z}_2 = -Q_{12} \cdot \mathrm{sign}(z_1 - \hat{p}) \cdot \sqrt{|z_1 - \hat{p}|} \\ \dot{z}_3 = z_4 + \boldsymbol{F}_{12}(\boldsymbol{\omega}) + \boldsymbol{G}_{12}(\boldsymbol{\omega})\boldsymbol{u} - Q_{21}(z_3 - \hat{q}) \\ \dot{z}_4 = -Q_{22} \cdot \mathrm{sign}(z_3 - \hat{q}) \cdot \sqrt{|z_3 - \hat{q}|} \\ \dot{z}_5 = z_6 + \boldsymbol{F}_{13}(\boldsymbol{\omega}) + \boldsymbol{G}_{13}(\boldsymbol{\omega})\boldsymbol{u} - Q_{31}(z_5 - \hat{r}) \\ \dot{z}_6 = -Q_{32} \cdot \mathrm{sign}(z_5 - \hat{r}) \cdot \sqrt{|z_5 - \hat{r}|} \end{cases} \tag{26}$$

where $z = \widehat{\xi}$, $\widehat{p}$, $\widehat{q}$ $\widehat{r}$ are the reconstructed angular rate sig-

nals. $\boldsymbol{Q}$ is the observer gain matrix with three rows and two columns. The convergence analysis of ESO_a is as given in [18,19]. Finally, the actuator faults can be estimated as

$$\widehat{\boldsymbol{f}_a} = \boldsymbol{G}_1^{-1}(\boldsymbol{\eta}) \cdot \begin{bmatrix} z_2 & z_4 & z_6 \end{bmatrix}^{\mathrm{T}} \tag{27}$$

3.3 Design of NDI_{ω}

NDI_{ω} is for angular rate control. The design of NDI_{ω} is based on the signal reconstruction and fault estimation. It can be described in the following steps:

Step 1 Calculate tracking error of angular rates.

$$\boldsymbol{e}_{\omega} = \boldsymbol{\omega}_c - \widehat{\boldsymbol{\omega}} \tag{28}$$

Step 2 Calculate desired derivatives of angular rates according to proportion-integral-derivative (PID) rules.

$$\dot{\boldsymbol{\omega}}_d = k_{p1}\boldsymbol{e}_{\omega} + k_{i1}\int_0^t \boldsymbol{e}_{\omega}\mathrm{d}t + k_{d1}\frac{\mathrm{d}\boldsymbol{e}_{\omega}}{\mathrm{d}t} \tag{29}$$

where k_{p1}, k_{i1}, and k_{d1} are PID gains.

Step 3 Let the desired derivatives equal to the true derivatives.

$$\dot{\boldsymbol{\omega}} = \dot{\boldsymbol{\omega}}_d \tag{30}$$

Step 4 Substitute (12) into (30).

$$\boldsymbol{F}_1(\boldsymbol{\omega}) + \boldsymbol{G}_1(\boldsymbol{\omega})(\boldsymbol{u}_c + \boldsymbol{f}_a) = \dot{\boldsymbol{\omega}}_d \tag{31}$$

Step 5 Transform (31), and replace $\boldsymbol{\omega}$ and $\boldsymbol{f}_a$ with $\widehat{\boldsymbol{\omega}}$ and $\widehat{\boldsymbol{f}_a}$ respectively.

$$\boldsymbol{u}_c = \boldsymbol{G}_1^{-1}(\boldsymbol{\omega}) \cdot (\dot{\boldsymbol{\omega}}_d - \boldsymbol{F}_1(\boldsymbol{\omega})) - \widehat{\boldsymbol{f}_a} \tag{32}$$

3.4 Design of NDI_{η}

NDI_{η} is for attitude control. The design of NDI_{η} can be described as following steps:

Step 1 Calculate tracking error of attitude angles.

$$\boldsymbol{e}_{\eta} = \boldsymbol{\eta}_c - \boldsymbol{\eta} \tag{33}$$

Step 2 Calculate desired derivatives of attitude angles according to PID rules.

$$\dot{\boldsymbol{\eta}}_d = k_{p2}\boldsymbol{e}_{\eta} + k_{i2}\int_0^t \boldsymbol{e}_{\eta}\mathrm{d}t + k_{d2}\frac{\mathrm{d}\boldsymbol{e}_{\eta}}{\mathrm{d}t} \tag{34}$$

where k_{p2}, k_{i2}, and k_{d2} are PID gains.

Step 3 Let desired derivatives equal to true derivatives.

$$\dot{\boldsymbol{\eta}} = \dot{\boldsymbol{\eta}}_d \tag{35}$$

Step 4 Substitute (13) into (35).

$$\boldsymbol{G}_2(\boldsymbol{\eta})\boldsymbol{\omega} = \dot{\boldsymbol{\eta}}_d \tag{36}$$

Step 5 Transform (36), and replace $\boldsymbol{\omega}$ with $\boldsymbol{\omega}_c$.

$$\boldsymbol{\omega}_c = \boldsymbol{G}_2^{-1}(\boldsymbol{\eta}) \cdot \dot{\boldsymbol{\eta}}_d \tag{37}$$

4. Simulation analysis

The simulations are carried out on a Cessna172 aircraft, cruising at the height of 500 m and at the speed of 50 m/s. The aircraft model is established based on (12) and (13), with reference to [29] and [30].

4.1 Scenario A: angular rate tracking control

In Scenario A, the ESO-NDI-based FTC scheme is compared with normal NDI to verify the feasibility and fault tolerant ability of ESO-NDI-based FTC proposed in this paper. The faults are set as (38) to (40).

$$\boldsymbol{f}_a = \begin{cases} -0.2\boldsymbol{u}_c, & t > 5 \\ \boldsymbol{0}, & t \leqslant 5 \end{cases} \tag{38}$$

$$f_p = f_q = f_r = \begin{cases} 0.05, & 10 < t < 20 \\ 0, & \text{otherwise} \end{cases} \tag{39}$$

$$\boldsymbol{f}_s = \begin{bmatrix} f_p & f_q & f_r \end{bmatrix}^{\mathrm{T}} \tag{40}$$

The control parameters are set as follows:

$$\boldsymbol{Q} = \begin{bmatrix} 10 & 3 \\ 10 & 3 \\ 10 & 3 \end{bmatrix}, \tag{41}$$

$$\boldsymbol{R} = \begin{bmatrix} 10 & 5 \\ 10 & 5 \\ 10 & 5 \end{bmatrix}, \tag{42}$$

$$\begin{cases} k_{p1} = 10 \\ k_{i1} = 0 \\ k_{d1} = 0 \end{cases}. \tag{43}$$

Angular rate responses under simultaneous sensor and actuator faults are shown in the following:

Fig. 3 gives the comparison of angular rate tracking results based on the FTC proposed in this paper and conventional ESO-NDI design in [16] or [17]. At the beginning the tracking results of proposed FTC have error in pitch rate channel due to the initial value error of ESO_s, but the error diminishes in two seconds. At 5 s, actuator faults cause tracking error in pitch rate channel, and both methods have eliminated the influence of actuator fault. After 10 s, the sensor fault occurred. It can be seen that conventional ESO-NDI design failed to follow the command, while the proposed FTC eliminate the influence of sensor faults and follows the command well. The comparison shows that conventional ESO-NDI design cannot deal with sensor faults, while the proposed FTC scheme can deal the simultaneous sensor and actuator faults, which means it has better fault tolerant ability.

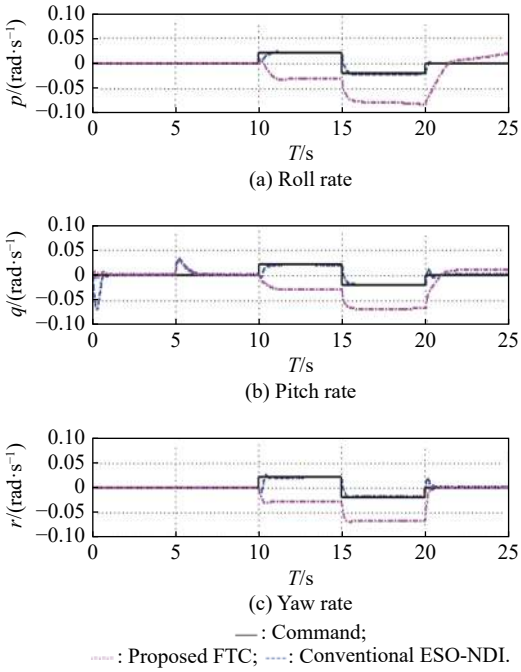

Fig. 3 Angular rate tracking responses

Fig. 4 gives the angular rate signal reconstruction results. At the beginning, the initial value error caused some error, but it soon diminished. At 10 s and 20 s, the measurement suddenly changed and caused reconstruction error, but the reconstruction soon get close to the true value, which shows the effectiveness of the signal reconstruction.

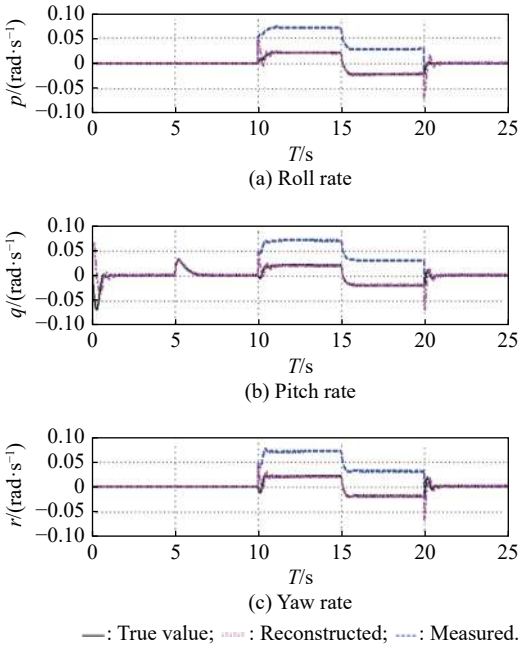

Fig. 4 Angular rate signal reconstruction results

4.2 Scenario B: attitude tracking control

In Scenario B, the attitude tracking response is given. The faults are set as (44) to (48).

$$\boldsymbol{f}_a = \begin{cases} -0.3\boldsymbol{u}_c, & t > 5 \\ \boldsymbol{0}, & t \leqslant 5 \end{cases} \tag{44}$$

$$f_p = \begin{cases} 0, & t < 10 \\ 0.01t - 0.1, & 10 < t < 20 \\ 0.1, & 20 < t \end{cases} \tag{45}$$

$$f_q = \begin{cases} 0, & t < 15 \\ 0.01t - 0.15, & 15 < t < 25 \\ 0.1, & 25 < t \end{cases} \tag{46}$$

$$f_r = \begin{cases} 0, & t < 10 \\ 0.01t - 0.1, & 10 < t < 20 \\ 0.1, & 20 < t \end{cases} \tag{47}$$

$$\boldsymbol{f}_s = \begin{bmatrix} f_p & f_q & f_r \end{bmatrix}^{\mathrm{T}} \tag{48}$$

The parameters of ESO_a, ESO_s, and NDI_ω are set as (41) to (43). The parameters of NDI_η is given as follows:

$$\begin{cases} k_{p2} = 2 \\ k_{i2} = 0 \\ k_{d2} = 0 \end{cases}. \tag{49}$$

During 0−25 s in angular rate loop, conventional ESO-NDI design is used and after 25 s the proposed FTC is used. The simulation response are shown in the following:

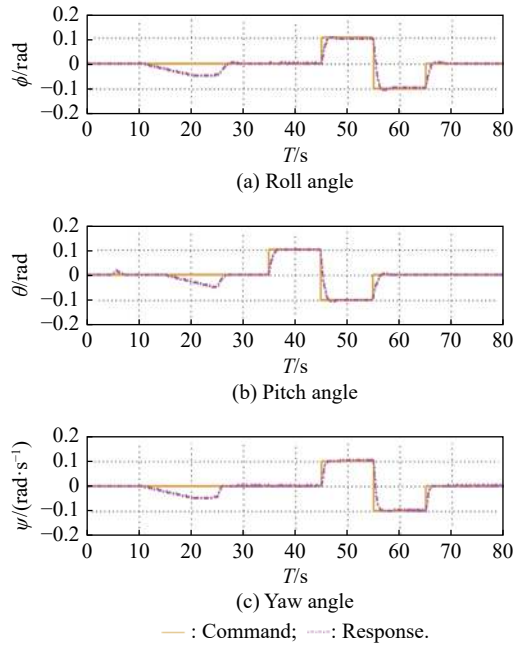

Fig. 5 Attitude tracking response

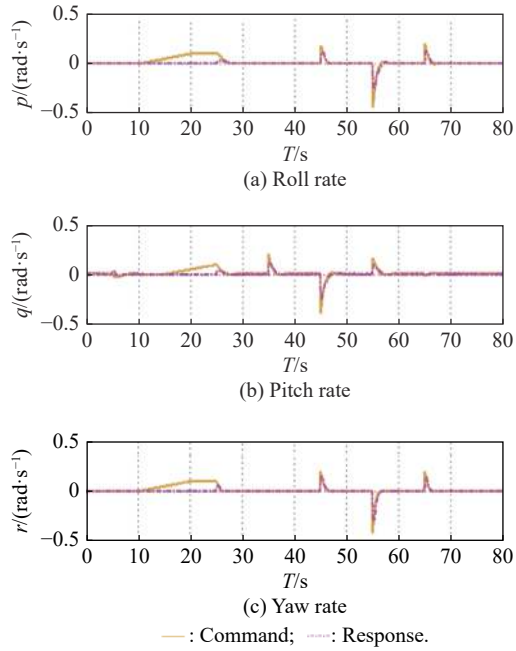

Fig. 6 Angular rate tracking response

It can be seen that sudden actuator faults at 5 s cause little tracking errors, but soon are eliminated. During 10−25 s, sensor faults cause tracking error in angular rate loop and attitude loop, and huge attitude deviation is caused, which again shows conventional ESO-NDI design has difficulty in dealing with sensor faults. After 25 s, the proposed FTC was used. As a result, angular rates and Euler angles follows the command successfully, which proves the proposed FTC has the ability to deal with simultaneous sensor and actuator faults.

5. Conclusions

In this paper, an FTC scheme based on ESO and NDI for civil aircrafts with sensor and actuator faults is proposed. First, an ESO-based signal reconstruction is proposed to solve the sensor faults. Second, another ESO is designed to estimate actuator faults. The angular rate controller and attitude controller are designed by using NDI. In angular rate loop, the NDI is designed based on the signal reconstruction and the estimation of actuator faults. Simulation shows that this FTC scheme is feasible and has better fault tolerant ability than conventional ESO-NDI design in dealing with sensor faults. The future work will be focused on faults of different kinds of sensors and how to deal with sensor noises.

References

[1] ALWI H, EDWARDS C. An adaptive sliding mode differentiator for actuator oscillatory failure case reconstruction. Automatica, 2013, 49(6): 642–651.

[2] ALWI H, EDWARDS C. Robust actuator fault reconstruction for LPV systems using sliding mode observers. Proc. of the IEEE Conference on Decision and Control, 2010: 84−89.

[3] QUAN L. Sliding mode observer-based fault diagnosis for flight control systems. Nanjing: Nanjing University of Aeronautics and Astronautics, 2019. (in Chinese)

[4] LU P, KAPEN E, VISSER C, et al. Aircraft fault-tolerant trajectory control using incremental nonlinear dynamic inversion. Control Engineering Practice, 2016, 57(9): 126−141.

[5] CHENG H H, LIU S Q, MA X J. Neural network incremental nonlinear dynamic inversion-based trajectory tracking control of an aircraft with pilot mishandling. Journal of Aeronautics, Astronautics and Aviation, 2021, 53(1): 45–58.

[6] LEE H, SNYDER S, HOVAKIMYAN N. An adaptive unknown input observer for fault detection and isolation of aircraft actuator faults. Proc. of the American Institute of Aeronautics and Astronautics Guidance, Navigation, & Control Conference, 2015: 266−273.

[7] YU X, FU Y, ZHANG Y, et al. Fault-tolerant aircraft control based on self-constructing fuzzy neural networks and multivariable SMC under actuator faults. IEEE Trans. on Fuzzy Systems, 2018, 26(4): 2324–2325.

[8] WANG X D, LIU S Q, CHENG H H, et al. Stable inversion based fault-tolerant trajectory tracking control of civil aircrafts autolanding. Journal of Aeronautics, Astronautics and Aviation, 2020, 52(3): 229–250.

[9] LIU S Q, SANG Y J, WHIDBORNE J F. Adaptive sliding-mode-backstepping trajectory tracking control of underactuated airships. Aerospace Science and Technology, 2020, 97(1): 1–13.

[10] XU X G, WEI Z Y, REN Z, et al. Time-varying fault-tolerant formation tracking based cooperative control and guidance for multiple cruise missile systems under actuator failures and directed topologies. Journal of Systems Engineering and Electronics, 2019, 30(3): 587–600.

[11] XU X, JIANG Z, HU H S. Cascade ADRC-based fault-tolerant control for a PVTOL aircraft with potential actuator failures. International Journal of Modelling Identification and Control, 2017, 28(3): 212–218.

[12] GUO Y Y, JIANG B, ZHANG Y M. A novel robust attitude control for quadrotor aircraft subject to actuator faults and wind gusts. IEEE/CAA Journal of Automatica Sinica, 2018, 5(1): 292–230.

[13] SHANG W, TANG S J, GUO J, et al. Robust sliding mode control with ESO for dual-control missile. Journal of Systems Engineering and Electronics, 2016, 27(5): 1073–1082.

[14] LI R H, LI T S, BU R X, et al. Active disturbance rejection with sliding mode control based course and path following for underactuated ships. Mathematical Problems in Engineering, 2013(13): 1–9.

[15] YAN K, CHEN M, WU Q X, et al. Extended state observer-based sliding mode fault-tolerant control for unmanned autonomous helicopter with wind gusts. IET Control Theory and Applications, 2019, 13(10): 1500−1513.

[16] YUAN R Y, FAN G L, YI J Q. Robust attitude controller for unmanned aerial vehicle using dynamic inversion and extended state observer. Proc. of the 2nd International Conference on Intelligent Computation Technology and Automation, 2009: 850−853.

[17] FALCONI G P, HEISE H D, HOLZAPFEL F. Fault-tolerant

position tracking of a hexacopter using an extended state observer. Proc. of the 6th International Conference on Automation, Robotics and Applications, 2015: 550−556.

[18] ERAZO C, ANGULO F, OLIVAR G. Stability analysis of the extended state observers by Popov criterion. Theoretical & Applied Mechanics Letters, 2012, 2(7): 306–309.

[19] GUO B Z, ZHAO Z L. On the convergence of an extended state observer for nonlinear systems with uncertainty. System & Control Letters, 2011, 60(4): 420–430.

[20] EDWARDS C, TAN C P. Sensor fault tolerant control using sliding mode observers. Control Engineering Practice, 2006, 14(7): 897–908.

[21] XIA J, XU J J. Observer-based Sensor Fault Detection and Signal Reconstruction Method. Journal of Beijing University of Aeronautics and Astronautics, 2013, 39(11): 1529−1535. (in Chinese)

[22] JOHANSEN T A, CRISTOFARO A, SORENSEN K, et al. On estimation of wind velocity, angle-of-attack and sideslip angle of small UAVs using standard sensor. Proc. of the International Conference on Unmanned Aircraft Systems, 2015: 510−519.

[23] LI P H. Research on sensor information reconfiguration of the flight control system. Xi'an, China: Northwestern Polytechnical University, 2014. (in Chinese)

[24] CHEN F Y, NIU J, JIANG G Q. Nonlinear fault-tolerant control for hypersonic flight vehicle with multi-sensor faults. IEEE Access, 2018, 6(5): 427–436.

[25] YANG B J, SONG Z R. Reconfiguration of the Angle of Attack Signal in Disability of Sensors. Aeronautical Science & Technology, 2018, 29(8): 33-40. (in Chinese)

[26] LU P, EYKEREN L V, KAMPEN E V, et al. Adaptive Three-Step Kalman Filter for Air Data Sensor Fault Detection and Diagnosis. Journal of Guidance Control & Dynamics, 2015. DOI: 10.251411.G001313.

[27] LU P, KAMPEN E V, VISSER C D, et al. Nonlinear aircraft sensor fault reconstruction in the presence of disturbances validated by real flight data. Control Engineering Practice, 2016, 49(2): 112–128.

[28] LU P, KAMPEN E V, VISSER C D, et al. Framework for simultaneous sensor and actuator fault-tolerant flight control. Journal of Guidance, Control, and Dynamics, 2017, 40(8): 2127–2135.

[29] LIU S Q. Flight dynamics and control of modern aircrafts. 2nd Ed. Shanghai: Shanghai Jiao Tong University Press, 2018. (in Chinese)

[30] VADIVELU P , LAKSHMANAN D , NAVEEN R, et al. Numerical study on longitudinal control of cessna 172 skyhawk aircraft by tail arm length. Proc. of the Institute of Physics Conference Series Materials Science and Engineering, 2020, 764(1): 012026.

Biographies

MA Xinjian was born in 1996. He received his B.S. degree in Shanghai Jiao Tong University. He is now studying in Shanghai Jiao Tong University as a postgraduate student. His research interests include flight control and fault tolerant control.
E-mail: Espada@sjtu.edu.cn

LIU Shiqian was born in 1971. He received his Ph.D degree in Nanjing University of Science and Technology. He is now an associate professor in Shanghai Jiao Tong University. His research interests include flight control and fault tolerant control.
E-mail: liushiqian@sjtu.edu.cn

CHENG Huihui was born in 1993. She received his B.S. degree in fluid mechanics engineering in Jiangsu University. She is now studying in Shanghai Jiao Tong University as a postgraduate student in aeronautics engineering. Her research interests include flight control and fault tolerant control.
E-mail: chenghh@sjtu.edu.cn